Article

Hardware-in-the-loop Simulation Method for an Individual Motor Torque Control to Improve the Running Performance of the Independently Rotating Wheel Type Railway Vehicle

Yonho Cho [1, *]

[1] Smart System Team, Hyundai-Rotem Company, Korea; car_d99@naver.com
* Correspondence: car_d99@naver.com; Tel.: +82-31-596-9075

Abstract: In order to realize the tram's low-floor structure, most of the trams that have been recently introduced adopt an independently rotating wheelset. In the case of trains driving in two regions with different gauges, an independently rotating wheelset may be applied to utilize the variable track technology. Since the independent rotation type wheelset has no rotational restraint of the left and right wheels, the difference in rotational speed between the outer and inner wheels occurs naturally during curved driving, and it is applied to railroad vehicles traveling in steep curve sections because it smoothly drives curved driving. However, the longitudinal creep force and the lateral restoring force are weakened as the left and right rotational constraints disappear. Lack of transverse direction restoring force weakens stability while causing continuous flange contact driving or zigzag phenomenon against disturbance. Under the conditions of driving in a steep curve, these railway vehicles generate excessive wear, noise, and lateral pressure, as well as deterioration of ride comfort and derailment. In order to overcome these drawbacks, a method has been proposed in which the torque of a motor mounted on each wheel is individually controlled to generate lateral restoring force or to improve driving performance through lateral displacement control using a yaw moment. In this paper, development using HILs was performed to check the performance and stability of the individual motor torque control technology before verifying by applying the individual motor torque control to the actual vehicle. HILs were constructed by combining a real-time dynamic analysis model of a railway vehicle with a drive motor to which real individual motor control was applied. Under the conditions of driving the test track where the actual test vehicle was tested, the analysis of the driving characteristics and the control characteristics of the disturbance was performed to confirm the proposed individual motor torque control performance.

Keywords: IRWs (Independently Rotating Wheels); Railway; HILs (Hardware In the Loops Simulation); ITC (Individual Torque Control); TRAM; Motor Control

1. Introduction

The independently rotating wheelset can make the low floor structure of the vehicle by eliminating the axle connecting the left and right wheels. The recently introduced tram is introducing a 100% low-floor vehicle to take care of the transportation handicapped persons. Since the rotational restraint force between the left and right wheel disappears, a rotational speed difference between the inner and outer wheels occurs during a curved driving, which enables natural curved driving. However, the longitudinal creep force and the lateral restoring force, which are inherent characteristics of the railway vehicle generated by the left and right wheel restraint,

disappear. Because of the lack of resilience against disturbances, continual flange contact or zigzag repeatedly impacting the left and right flanges may occur [1,2]. In the case of a driving bogie using a motor mounted on each wheel, this disadvantage can be improved through individual torque control. When the sharp curve driving performance is improved through the application of individual motor torque control, it is possible to reduce noise and wear by improving the driving performance while driving the steep curve of 15 mR or less. It is possible to plan routes with high profitability and high operational efficiency through the densely populated areas in the city center or through key commercial areas. This paper describes the technology verification using HILs composed by connecting a real-time vehicle analysis model and a motor to which a real individual torque is applied before performing a driving test by applying the individual motor torque control (ITC) of the developed independent driving wheelset to a real vehicle. The real-time vehicle analysis model was developed based on the modified dynamic model of the independently rotating railway vehicle proposed by cho and kwack [3]. In order to perform verification of the developed individual motor control technology, a miniature driving test stand was produced, and Ahn, Oh, and Won were verified through various developed algorithms through a test using the manufactured miniature driving test stand [4,5,6]. Various individual motor control technologies for improving the performance of independent rotating railroad vehicles have been developed through simulations and miniature tests as research subjects of many researchers such as Mei, Dukkipati, Goodall, Perez, etc [7,8,9,10,11,12,13].

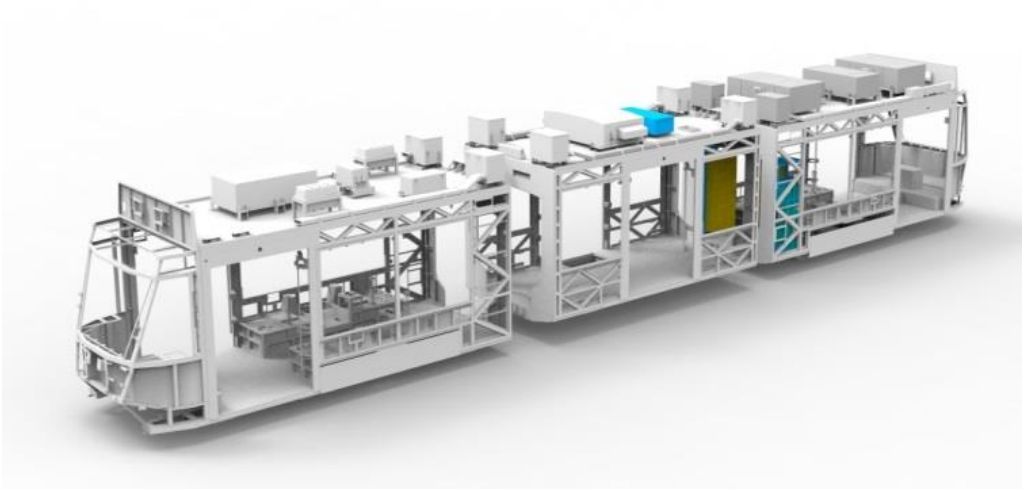

Figure 1. Test vehicle applied with developed ITC technology

2. HILs Configurations

HILs has been developed and used for the purpose of reducing the risk in the nuclear industry and the aerospace industry, where it is difficult to manufacture actual test vehicles. In addition, HILs is widely used in various industries because it can perform evaluation of various test conditions with high reliability in a short time [14,15,16,17,18,19]. Due to the reliability of HILs and the shortening of the development period, the most research cases in the automotive industry have been published [20,21,22,23,24,25,26,27,28,29,30,31]. As the automobile industry is advanced, various control functions are added and HILs is the most widely applied industrial field to reflect it in products. In the case of railroad vehicles, HIls has been actively applied to reduce the risk of developing new technologies and applying them to actual vehicles to verify performance [32,33,34].

HILs are often used to evaluate real-world development or controller prototypes using fast computing devices and highly reliable real-time analysis models. To construct HILs for verification of individual motor torque control technology to improve the driving performance of railroad vehicles using the independently rotating wheelset proposed in this paper, it is necessary to secure highly reliable real-time vehicle analysis model. MILs (Model In the Loop simulation) for real-time evaluation

by applying a control algorithm to an analytical model for a real-time analysis model, SILs (Software In the Loop simulation) for evaluating software by coding a control algorithm, and real-time development parts or objects It is also classified and used in HILs (Hardware in the Loop simulation), which is evaluated in connection with an analytical model.

In this paper, the development of a highly reliable real-time analysis model and the hardware configuration capable of real-time calculation are described, and HILs are constructed by preparing individual motors and individual motor controllers to be applied to test vehicles in advance. The analysis model was composed of 26 degrees of freedom model based on Matlab, and HILS was constructed using dSPace's Scalexio platform, which is the fastest and most reliable in HILs configuration.

2.1. Real-time analysis model

The test vehicle consists of a three-car combination as shown in Figure 1. The driving bogies are applied to the leading vehicle and the trailer bogies are applied to the rear vehicle. The inter

mediate vehicle is bound to the front and rear vehicles with a coupler and operates in the air. In general, a 5-car tram that is in operation is a three-bogies support system, and the test vehicle proposed in this paper is designed to perform a function equivalent to 1/2 of a 5-module standard vehicle. The developed system can be applied to three-car trains as well as five-car trains.

In the driving bogie, the clearance between the motor and the driving gear is limited, so the desired steering angle cannot be applied when driving a sharp curve. On the other hand, since the trailer bogie is not equipped with a motor, a steering device can be applied to apply a steering angle equivalent to a radial steering when driving a sharp curve. Active steering control can be applied to the trailer bogie, but since driving bogie is difficult to apply to the active steering control, individual motor torque control technology using motor torque control has been developed.

In this paper, in order to verify the individual motor torque control technology applied to the driving bogie using HILS, the 26-degree real-time test of a three-car train test vehicle that adds rotational freedom of the left and right wheels to apply control torque to each wheel of the drive bogie An analytical model was developed. The real-time analysis model linearizes most of the nonlinear elements to enable quick calculation without compromising the accuracy of the analysis, and simplifies the real-time analysis model with equations (1) to (26) through some assumptions. Figure 2 and Figure 3 are analysis model of a test vehicle for real-time analysis model development. When the analysis is performed by considering the three vehicles as a three-section link, it is possible to obtain an analytically correct solution, but it is difficult to guarantee real-time analysis because the formula is complicated and the amount of calculation is increased. In this paper, instead of the link structure, the lateral stiffness model for the joint is added to simplify the equation to predict the behavior of the three-dimensional analysis model as a resultant force model. Six motion equations were derived, taking into account only the degrees of freedom for lateral displacement and yaw displacement for a three-car body. The equations of motion for bogies and wheelsets are independent of vehicle organization, so the motion equations for the analysis of the curves of the existing independent drive railroad vehicles have been applied.

A real-time analysis model was developed to perform the steering performance verification analysis of the test vehicle using HILs. After creating an analysis model using Simulink for a 26-degree-of-freedom analysis model consisting of 4 wheelsets, 2 bogies, and 3 car bodies, it was confirmed that the analysis was normally performed by performing continuous time analysis using a variable step integrator. dSPACE's SCALEXIO computation equipment being introduced for real-time analysis guarantees real-time analysis performance up to an integral step of 10 microseconds with discrete time analysis. By performing the discrete time analysis using a fixed step integrator on the program created using the developed analysis model, it was confirmed that the analysis is normally performed under the condition that the integration step is greater than 10 microseconds.

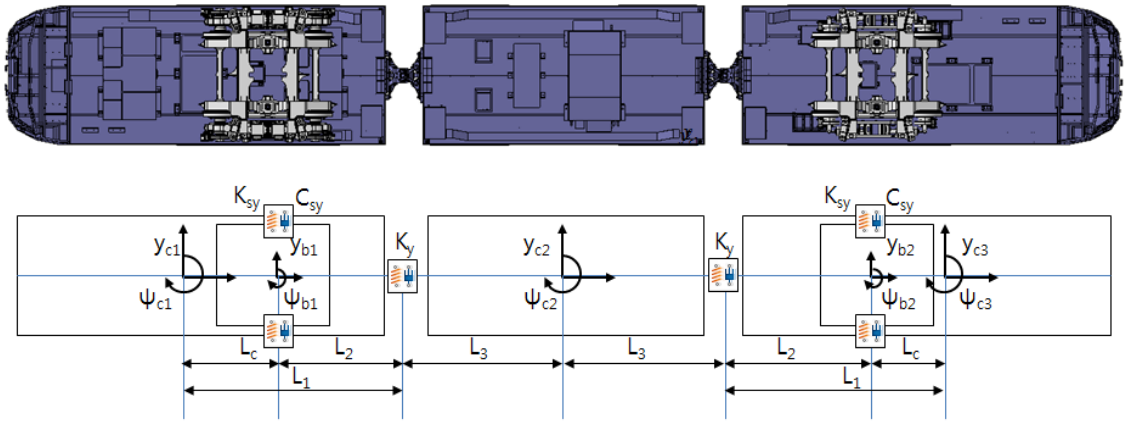

Figure 2. Three-car body test vehicle connected by an inter-body spring model

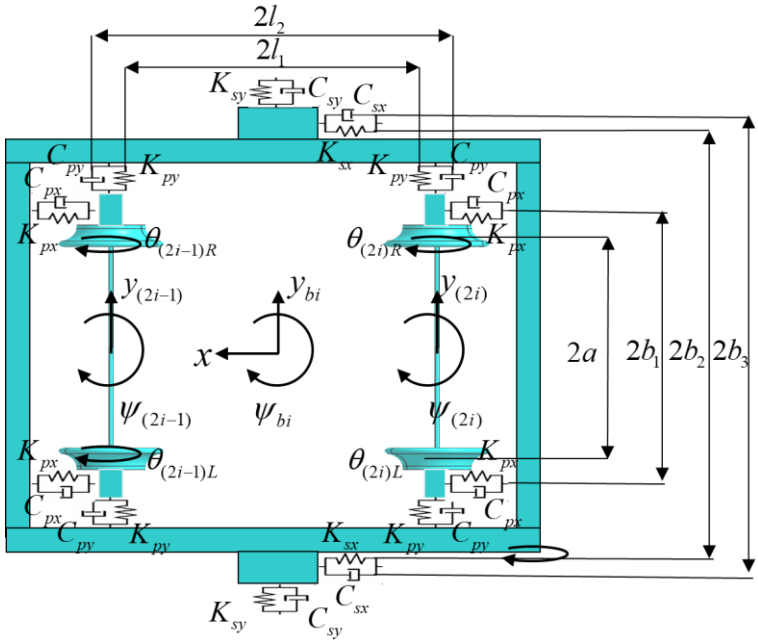

Figure 3. Bogie analysis model including independently rotating wheelset (Leading bogie i=1, Trailer bogie i=2)

- Carbody equations

$$m_{c1}\ddot{y}_{c1} = 2K_{sy}y_{b1} - 2K_{sy}y_{c1} + 2C_{sy}\dot{y}_{b1} - 2C_{sy}\dot{y}_{c1} - 2K_{sy}L_c\psi_{c1} \\ -2C_{sy}L_c\dot{\psi}_{c1} - K_y y_{c1} + K_y y_{c2} - K_y L_1\psi_{c1} - K_y L_3\psi_{c2} \quad (1)$$

$$m_{c2}\ddot{y}_{c2} = K_y y_{c1} - 2K_y y_{c2} + K_y y_{c3} + K_y L_1\psi_{c1} - K_y L_1\psi_{c3} \quad (2)$$

$$m_{c3}\ddot{y}_{c3} = -2K_{sy}y_{c3} + 2K_{sy}y_{b2} - 2C_{sy}\dot{y}_{c3} + 2C_{sy}\dot{y}_{b2} - 2K_{sy}L_c\psi_{c3} \\ -2C_{sy}L_c\dot{\psi}_{c3} + K_y y_{c2} - K_y y_{c3} + K_y L_3\psi_{c2} + K_y L_1\psi_{c3} \quad (3)$$

$$I_{cz1}\ddot{\psi}_{c1} = -2K_{sy}L_c^2\psi_{c1} - 2C_{sy}L_c^2\dot{\psi}_{c1} - 2K_{sx}L_1^2\psi_{c1} - 2C_{sx}L_3^2\dot{\psi}_{c1} + 2K_{sx}L_1^2\psi_{b1} + 2C_{sx}L_3^2\dot{\psi}_{b1} + 2K_{sy}L_c y_{b1} + 2C_{sy}L_c\dot{y}_{b1} + C_{sy}L_2\dot{y}_{c1} + K_{sy}L_2 y_{c1} + K_y L_1 y_{c2} - K_y L_1 y_{c1} - K_y L_1^2\psi_{c1} - K_y L_1 L_3\psi_{c2} \quad (4)$$

$$I_{cz2}\ddot{\psi}_{c2} = -K_y L_3 y_{c1} + K_y L_3 y_{c3} - K_y L_1 L_3\psi_{c1} - 2K_y L_3^2\psi_{c2} - K_y L_1 L_3\psi_{c3} \quad (5)$$

$$I_{cz3}\ddot{\psi}_{c3} = -2K_{sy}L_c^2\psi_{c3} - 2C_{sy}L_c^2\dot{\psi}_{c3} - 2K_{sx}L_1^2\psi_{c3} - 2C_{sx}L_3^2\dot{\psi}_{c3} + 2K_{sx}L_1^2\psi_{b2} + 2C_{sx}L_3^2\dot{\psi}_{b2} - 2K_{sy}L_c y_{b2} - 2C_{sy}L_c\dot{y}_{b2} - C_{sy}L_2\dot{y}_{c3} - K_{sy}L_2 y_{c3} - K_y L_1 y_{c2} + K_y L_1 y_{c3} - K_y L_1^2\psi_{c3} - K_y L_1 L_3\psi_{c2} \quad (6)$$

- Front wheelset equations of leading bogie

$$m_w\ddot{y}_1 = (-\frac{w\lambda}{a} - 2K_{py})y_1 + (\frac{-2f_{11}}{v} - \frac{-2f_{11}}{v}\frac{r_0}{a}\lambda - 2C_{py})\dot{y}_1 + 2f_{11}\psi_1 - \frac{2f_{12}}{v}\dot{\psi}_1 + 2K_{py}y_{b1} + 2C_{py}\dot{y}_{b1} + 2K_{py}l_1\psi_{b1} + 2C_{py}l_2\dot{\psi}_{b1} \quad (7)$$

$$I_{wz}\ddot{\psi}_1 = -2a\frac{\lambda}{r_0}f_{33}y_1 + (\frac{2f_{12}}{v} - I_y\frac{v}{r_0}\frac{\lambda}{a} + 2f_{12}\frac{r_0}{v}\frac{\lambda}{a})\dot{y}_1 + (-2f_{12} + a\lambda w - 2K_{px}b_1^2)\psi_1 + (-2a^2\frac{f_{33}}{v} - \frac{2f_{22}}{v} - 2C_{px}b_1^2)\dot{\psi}_1 + f_{33}a\frac{r_0}{v}\dot{\theta}_{1L} - f_{33}a\frac{r_0}{v}\dot{\theta}_{1R} + 2K_{px}b_1^2\psi_{b1} + 2C_{px}b_1^2\dot{\psi}_{b1} \quad (8)$$

$$I_{w1}\ddot{\theta}_{1L} = f_{33}\lambda y_1 + r_0 f_{33}\frac{a}{v}\dot{\psi}_1 - f_{33}\frac{r_0^2}{v}\dot{\theta}_{1L} \quad (9)$$

$$I_{w1}\ddot{\theta}_{1R} = -f_{33}\lambda y_1 - r_0 f_{33}\frac{a}{v}\dot{\psi}_1 - f_{33}\frac{r_0^2}{v}\dot{\theta}_{1R} \quad (10)$$

- Rear wheelset equations of leading bogie

$$m_w\ddot{y}_2 = (-\frac{w\lambda}{a} - 2K_{py})y_2 + (\frac{-2f_{11}}{v} - \frac{-2f_{11}}{v}\frac{r_0}{a}\lambda - 2C_{py})\dot{y}_2 + 2f_{11}\psi_2 - \frac{2f_{12}}{v}\dot{\psi}_2 + 2K_{py}y_{b1} + 2C_{py}\dot{y}_{b1} - 2K_{py}l_1\psi_{b1} - 2C_{py}l_2\dot{\psi}_{b1} \quad (11)$$

$$I_{wz}\ddot{\psi}_2 = -2a\frac{\lambda}{r_0}f_{33}y_2 + (\frac{2f_{12}}{v} - I_y\frac{v}{r_0}\frac{\lambda}{a} + 2f_{12}\frac{r_0}{v}\frac{\lambda}{a})\dot{y}_2 + (-2f_{12} + a\lambda w - 2K_{px}b_1^2)\psi_2 + (-2a^2\frac{f_{33}}{v} - \frac{2f_{22}}{v} - 2C_{px}b_1^2)\dot{\psi}_2 + f_{33}a\frac{r_0}{v}\dot{\theta}_{2L} - f_{33}a\frac{r_0}{v}\dot{\theta}_{2R} + 2K_{px}b_1^2\psi_{b1} + 2C_{px}b_1^2\dot{\psi}_{b1} \quad (12)$$

$$I_{w2}\ddot{\theta}_{2L} = f_{33}\lambda y_2 + r_0 f_{33}\frac{a}{v}\dot{\psi}_2 - f_{33}\frac{r_0^2}{v}\dot{\theta}_{2L} \quad (13)$$

$$I_{w2}\ddot{\theta}_{2R} = -f_{33}\lambda y_2 - r_0 f_{33}\frac{a}{v}\dot{\psi}_2 - f_{33}\frac{r_0^2}{v}\dot{\theta}_{2R} \quad (14)$$

- Leading bogie equations

$$m_b\ddot{y}_{b1} = 2K_{py}y_1 + 2C_{py}\dot{y}_1 + 2K_{py}y_2 + 2C_{py}\dot{y}_2 + (-4K_{py} - 2K_{sy})y_{b1} + (-4C_{py} - 2C_{sy})\dot{y}_{b1} \tag{15}$$

$$I_b\ddot{\psi}_{b1} = 2K_{py}l_1y_1 + 2C_{py}l_2\dot{y}_1 + 2K_{px}b_1^2\psi_1 + 2C_{px}b_1^2\dot{\psi}_1 - 2K_{py}l_1y_2 - 2C_{py}l_2\dot{y}_2 + 2K_{px}b_1^2\psi_2 + 2C_{px}b_1^2\dot{\psi}_2 + (-4K_{py}l_1^2 - 4K_{px}b_1^2 - 2K_{sx}b_2^2)\psi_{b1} + (-4C_{py}l_2^2 - 4C_{px}b_1^2 - 2C_{sx}b_3^2)\dot{\psi}_{b1} \tag{16}$$

- Front wheelset equations of trailer bogie

$$m_w\ddot{y}_3 = (-\frac{w\lambda}{a} - 2K_{py})y_3 + (\frac{-2f_{11}}{v} - \frac{-2f_{11}}{v}\frac{r_0}{a}\lambda - 2C_{py})\dot{y}_3 + 2f_{11}\psi_3 - \frac{2f_{12}}{v}\dot{\psi}_3 + 2K_{py}y_{b2} + 2C_{py}\dot{y}_{b2} + 2K_{py}l_1\psi_{b2} + 2C_{py}l_2\dot{\psi}_{b2} \tag{17}$$

$$I_{wz}\ddot{\psi}_3 = -2a\frac{\lambda}{r_0}f_{33}y_3 + (\frac{2f_{12}}{v} - I_y\frac{v}{r_0}\frac{\lambda}{a} + 2f_{12}\frac{r_0}{v}\frac{\lambda}{a})\dot{y}_3 + (-2f_{12} + a\lambda w - 2K_{px}b_1^2)\psi_3 + (-2a^2\frac{f_{33}}{v} - \frac{2f_{22}}{v} - 2C_{px}b_1^2)\dot{\psi}_3 + f_{33}a\frac{r_0}{v}\dot{\theta}_{3L} - f_{33}a\frac{r_0}{v}\dot{\theta}_{3R} + 2K_{px}b_1^2\psi_{b2} + 2C_{px}b_1^2\dot{\psi}_{b2} \tag{18}$$

$$I_{w3}\ddot{\theta}_{3L} = f_{33}\lambda y_3 + r_0f_{33}\frac{a}{v}\dot{\psi}_3 - f_{33}\frac{r_0^2}{v}\dot{\theta}_{3L} \tag{19}$$

$$I_{w3}\ddot{\theta}_{3R} = -f_{33}\lambda y_3 - r_0f_{33}\frac{a}{v}\dot{\psi}_3 - f_{33}\frac{r_0^2}{v}\dot{\theta}_{3R} \tag{20}$$

- Rear wheelset equations of trailer bogie

$$m_w\ddot{y}_4 = (-\frac{w\lambda}{a} - 2K_{py})y_4 + (\frac{-2f_{11}}{v} - \frac{-2f_{11}}{v}\frac{r_0}{a}\lambda - 2C_{py})\dot{y}_4 + 2f_{11}\psi_4 - \frac{2f_{12}}{v}\dot{\psi}_4 + 2K_{py}y_{b2} + 2C_{py}\dot{y}_{b2} - 2K_{py}l_1\psi_{b2} - 2C_{py}l_2\dot{\psi}_{b2} \tag{21}$$

$$I_{wz}\ddot{\psi}_4 = -2a\frac{\lambda}{r_0}f_{33}y_4 + (\frac{2f_{12}}{v} - I_y\frac{v}{r_0}\frac{\lambda}{a} + 2f_{12}\frac{r_0}{v}\frac{\lambda}{a})\dot{y}_4 + (-2f_{12} + a\lambda w - 2K_{px}b_1^2)\psi_4 + (-2a^2\frac{f_{33}}{v} - \frac{2f_{22}}{v} - 2C_{px}b_1^2)\dot{\psi}_4 + f_{33}a\frac{r_0}{v}\dot{\theta}_{4L} - f_{33}a\frac{r_0}{v}\dot{\theta}_{4R} + 2K_{px}b_1^2\psi_{b2} + 2C_{px}b_1^2\dot{\psi}_{b2} \tag{22}$$

$$I_{w4}\ddot{\theta}_{4L} = f_{33}\lambda y_4 + r_0f_{33}\frac{a}{v}\dot{\psi}_4 - f_{33}\frac{r_0^2}{v}\dot{\theta}_{4L} \tag{23}$$

$$I_{w4}\ddot{\theta}_{4R} = -f_{33}\lambda y_4 - r_0f_{33}\frac{a}{v}\dot{\psi}_4 - f_{33}\frac{r_0^2}{v}\dot{\theta}_{4R} \tag{24}$$

- Trailer bogie equations

$$\begin{aligned} m_b\ddot{y}_{b2} &= 2K_{py}y_3 + 2C_{py}\dot{y}_3 + 2K_{py}y_4 + 2C_{py}\dot{y}_4 \\ &+ (-4K_{py} - 2K_{sy})y_{b2} + (-4C_{py} - 2C_{sy})\dot{y}_{b2} \end{aligned} \tag{25}$$

$$\begin{aligned} I_b\ddot{\psi}_{b1} &= 2K_{py}l_1y_1 + 2C_{py}l_2\dot{y}_1 + 2K_{px}b_1^2\psi_1 + 2C_{px}b_1^2\dot{\psi}_1 - 2K_{py}l_1y_2 - 2C_{py}l_2\dot{y}_2 \\ &+ 2K_{px}b_1^2\psi_2 + 2C_{px}b_1^2\dot{\psi}_2 + (-4K_{py}l_1^2 - 4K_{px}b_1^2 - 2K_{sx}b_2^2)\psi_{b1} \\ &+ (-4C_{py}l_2^2 - 4C_{px}b_1^2 - 2C_{sx}b_3^2)\dot{\psi}_{b1} \end{aligned} \tag{26}$$

2.2. Motor and motor controller for individual torque control

A permanent magnet synchronous motor (PMSM) with excellent torque control responsiveness was developed and applied to test vehicles. In order to secure the margin of the control torque excluding the driving force in the driving motor, the capacity was increased compared to the existing motor, and the specification was changed to a 60 kW class motor with excellent torque characteristics. (Existing PMSM is 45 kW)

The output characteristics of an ITC (Individual Torque Control) motor are shown in Figure 4. The maximum output occurs in a constant output range of 1400 rpm to 2400 rpm, and it exhibits high-speed characteristics in the range of 2400 rpm to 4450 rpm. The design was conducted based on three points of 500 Nm @ 1400 rpm, 290 Nm @ 2400 rpm, and 90 Nm @ 4450 rpm on the graph. The section views of the 45 kW class -Bar type IPMSM before the design change and the 60 kW class-U type IPMSM after the change are also displayed in Figure 5. The main design change was that the required torque increased by approximately 50% from 333 Nm @ 1400 rpm to 500 Nm @ 1400 rpm. As the sensing method of mounting the encoder on the outside was changed to the method of inserting the resolver into the motor, the stacking length effective for the motor output was reduced. Therefore, the design for improving the power should be considered.

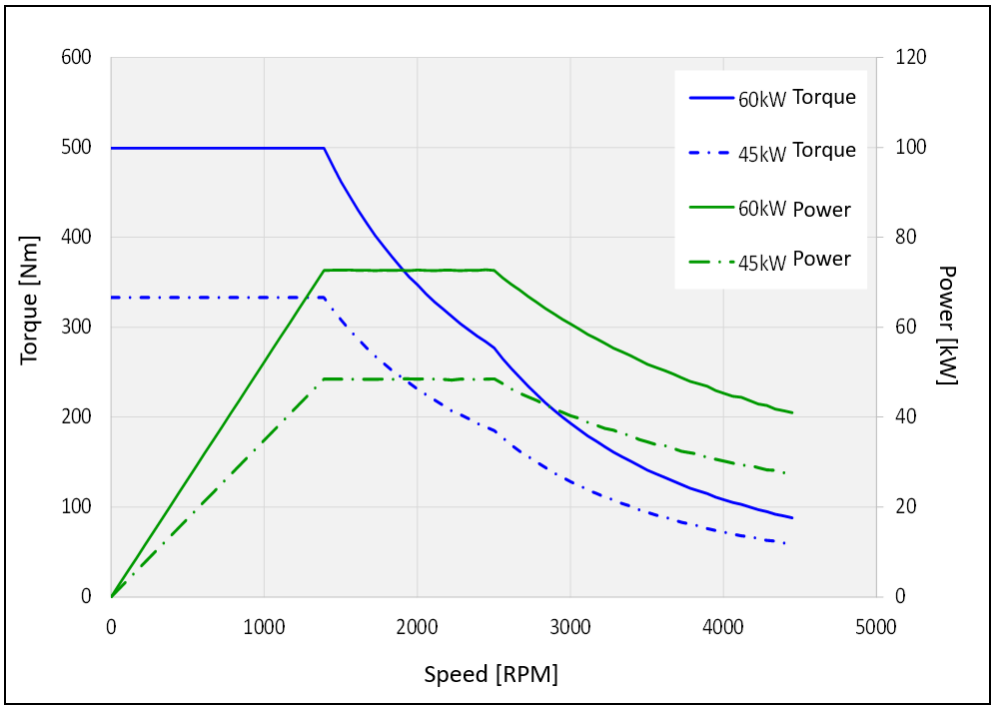

Figure 4. Comparison of the output specifications of the newly designed PMSM and the existing PMSM

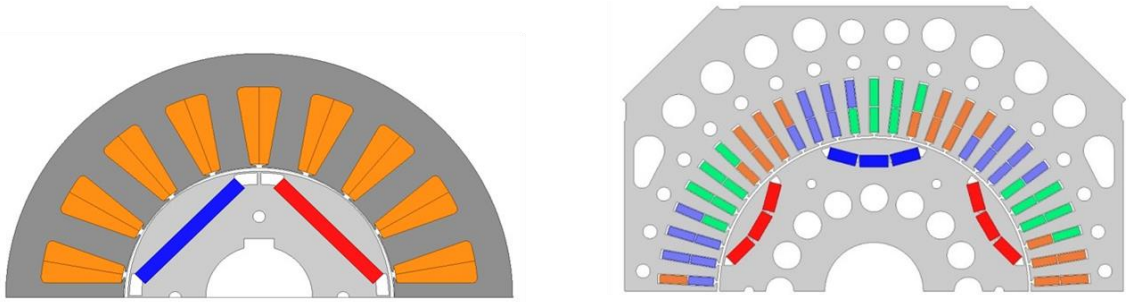

Figure 5. Left: 45 kW class -Bar type IPMSM, Right: 60 kW class-U type IPMSM

The pole-slot number combination of the motor was changed from 4 poles 18 slots to 6 poles 54 slots to improve torque and obtain sine counter electromotive force. The winding was designed as a square copper wire that can increase the area of the winding to improve the motor output in the existing circular wire. The permanent magnet type was changed to samarium-cobalt, which is superior in price and thermal properties to neodymium. Table 1 shows the major design changes of IPMSM.

Table 1. IPMSM Specification Comparison Table

Classification	45 kW class bar type IPMSM	60 kW class U type IPMSM
Output specifications	333 [Nm] @ 1400 [rpm]	500[Nm] @ 1400 [rpm]
Pole-slot	4 poles / 18 slots	6 poles / 54 slots
Volume	332*250 [mm]	350*150 [mm]
Winding	Circular	Square copper wire
Permanent magnet type	Neodymium	Samarium-cobalt
Location sensing	External mounting method (encoder)	Located inside the motor (resolver)
Torque control method	Driving / regeneration magnetic flux map	←
Switching frequency	4 k [Hz]	←
DC link voltage	750 [V]	←

As shown in Figure 6, the ITC motor torque has the characteristic of combining the driving / braking torque with a constant output of the general rail traction motor with the lateral displacement restoration torque, which has an average output of 0 but swings up and down. This requires high frequency torque response and high torque control performance.

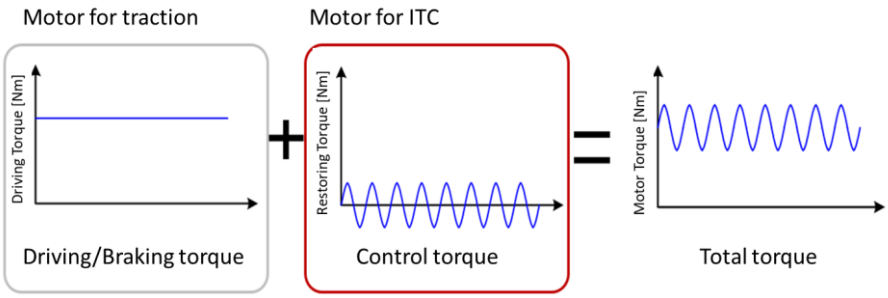

Figure 6. Torque characteristics of motor for ITC

2.3. Composition of HILs platform for verification of individual motor torque control

HILs replaces the test object with a virtual analysis model when it is difficult to secure the actual test object or when a risk is involved in the test, and the development part of interest is composed of a real product. It is possible to conduct product development and evaluation in a more realistic environment through testing using a mutual response relationship between a real product and a real-time virtual analysis model.

n this paper, to verify the performance of the lateral displacement control system using the individual motor torque control under development, an HILS environment was constructed and the controller performance was evaluated. The first thing to consider in establishing the HILS environment is the reliability and speed of calculation equipment. The HILS platform operating in the actual industrial field is mainly used by the platform using Opal-RT series, NI-PXI series, and dSPACE's Autobox. Although it is relatively expensive in high-tech industries such as automobiles and aviation, dSPACE's products are excellent in terms of reliability and computational speed. In this paper, considering this excellence, HILs using SCALEXIO, a successor to dSPACE's Autobox, was constructed.

In order to run dSPACE's SCALEXIO platform, a dedicated PC is required to run five types of software: Configuration desk, Control desk, Model desk, and Motion desk provided by Matlab of Mathworks and dSPACE. By adding a beam project to visualize the results of the motion desk that simulates the test results in real-time 3D graphics, an environment was built to perform the test while projecting it on a 100-inch screen to feel the driving of a real vehicle. The control PC and the SCALEXIO device are connected to each other through an Ethernet cable, and the SCALEXIO device is connected to the Hypertronic connector based on the predefined controller pin map information. In order to check the characteristics of the disturbance response to the real-time analysis model, a disturbance input device that generates two types of input signals, an acceleration sensor and a load cell, was separately manufactured and connected. By adding a CAN information-based remote operation device, the speed is varied or an emergency stop signal is generated, and the function of turning the controller ON / OFF through mechanical switching is added. Figure 7 shows the HILs system configured for ITC verification.

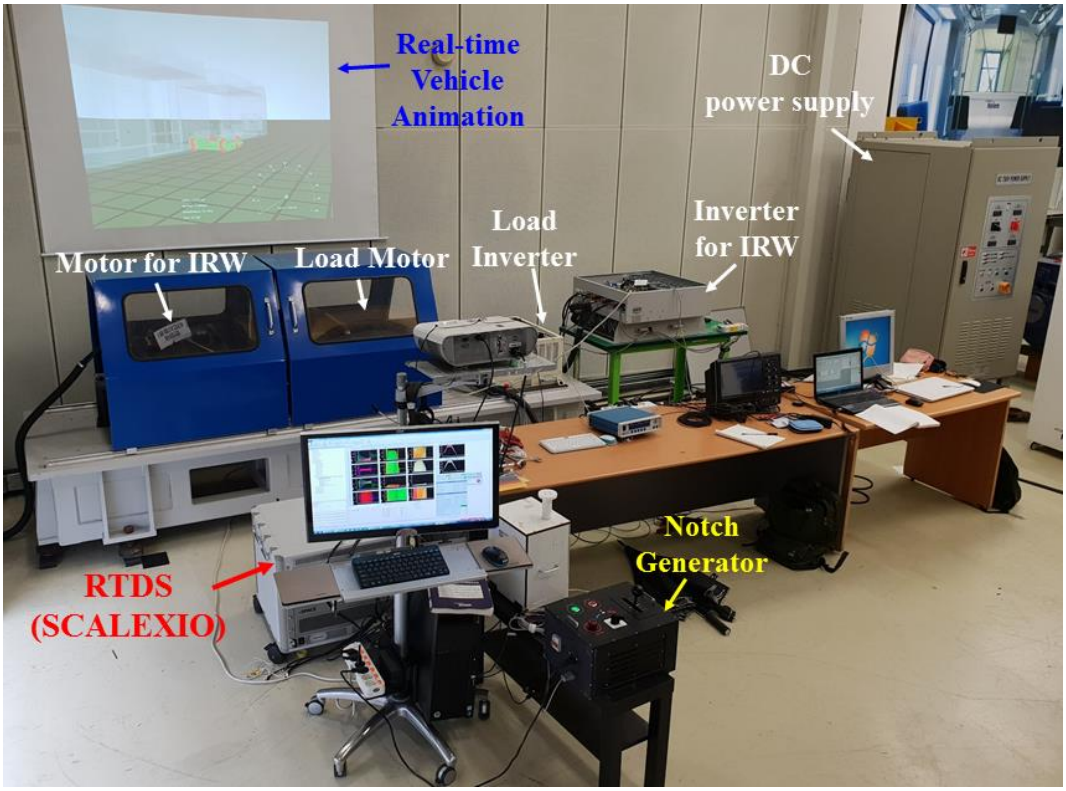

Figure 6. HILs system configured for ITC verification.

2.4. Establishment of controller verification HILs using dSPACE platform

In order to establish a HILS environment and perform full-scale testing, it is necessary to define a real-time driving analysis model to replace the actual test vehicle with Matlab / Simulink, and to define the analog output signal that converts the result of the analysis model into an electrical signal and delivers it to the controller. The controller that receives the sensor signal extracted from the virtual test vehicle sends the calculated torque information to the inverter. The actual driving torque generated by driving the motor by the inverter is measured and transmitted back to the real-time analysis model, so the closed loop must be completed. In order to complete this series of test procedures, it is necessary to develop a program using five software such as Matlab, configuration desk, control desk, model desk, and motion desk. Figure 7 and Figure 8 are conceptual diagrams of the motor configuration of a driving bogie to which individual motor torque control is applied. Three of the four motors of the driving cart are composed of a virtual model, and only one motor is configured with HILs to evaluate the controller by applying a real motor. The configuration desk defines input and output signals, and the control desk uploads the compiled model to SCALEXIO and performs setup and monitoring to perform virtual driving test. Finally, the virtual test vehicle implements the 3D shape output information using the motion desk.

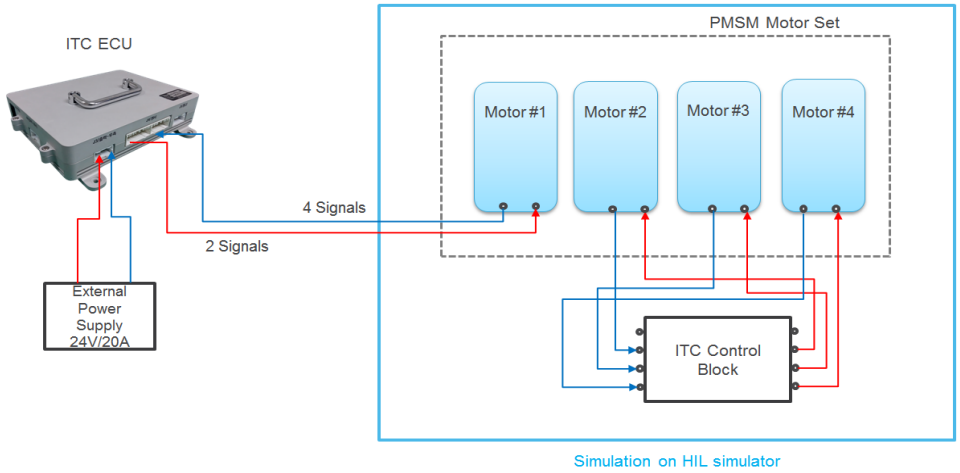

Figure 7. A conceptual diagram of the motor configuration for constructing a driving bogie to be applied to individual motor controllers in the HILs environment

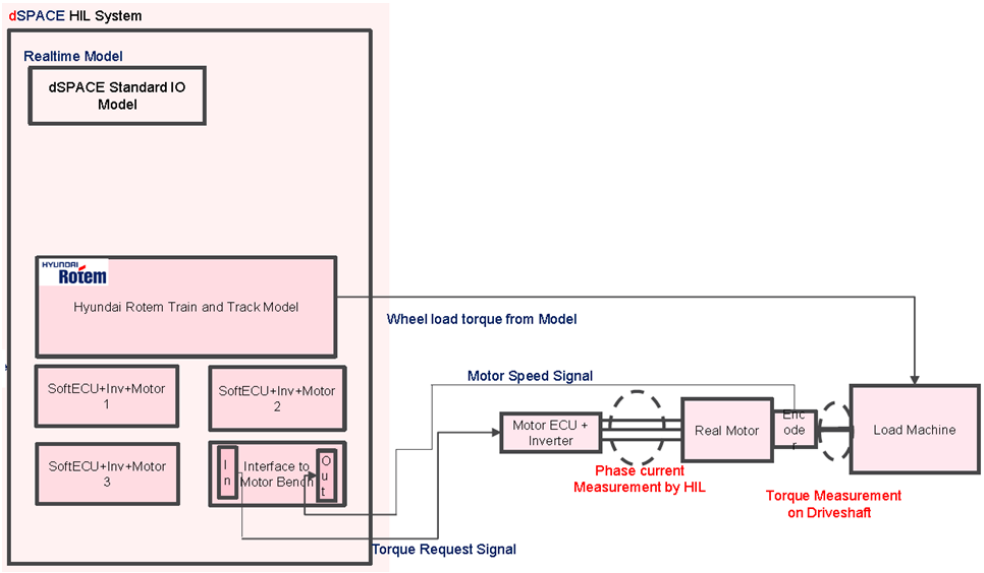

Figure 8. Virtual motor model and real motor signal connection configuration implemented in dSPACE platform

Figure 9 shows the definition of input / output relations for the measurement signals of 26 degrees of freedom real-time vehicle analysis model, 3 virtual motor models, and 1 real motor using the Configuration desk. Figure 10 shows various results calculated from the real-time analysis model on the control desk and measured signal values in a graph. In addition, various control input values are defined and monitored to control the actual controller and the virtual controller. Figure 11 shows the motion desk window that finally represents the performance of the virtual vehicle reflecting the driving characteristics of the controller and the actual motor in a test environment in a 3D graph.

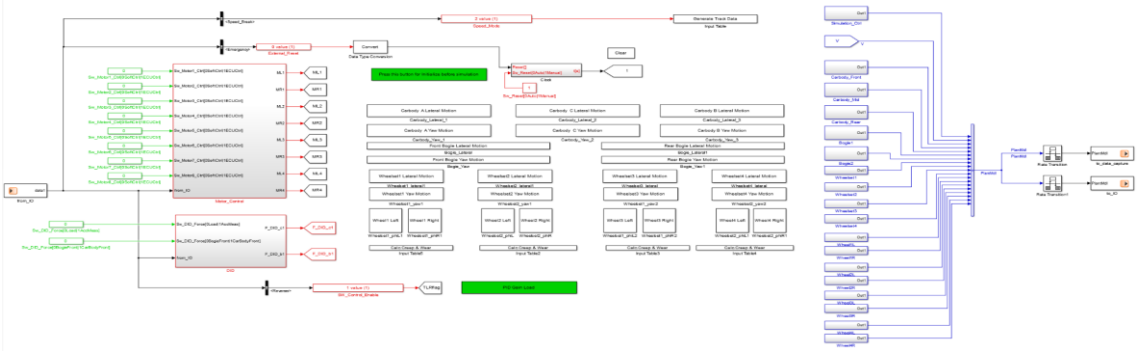

Figure 9. I / O signal definition using Configuration desk

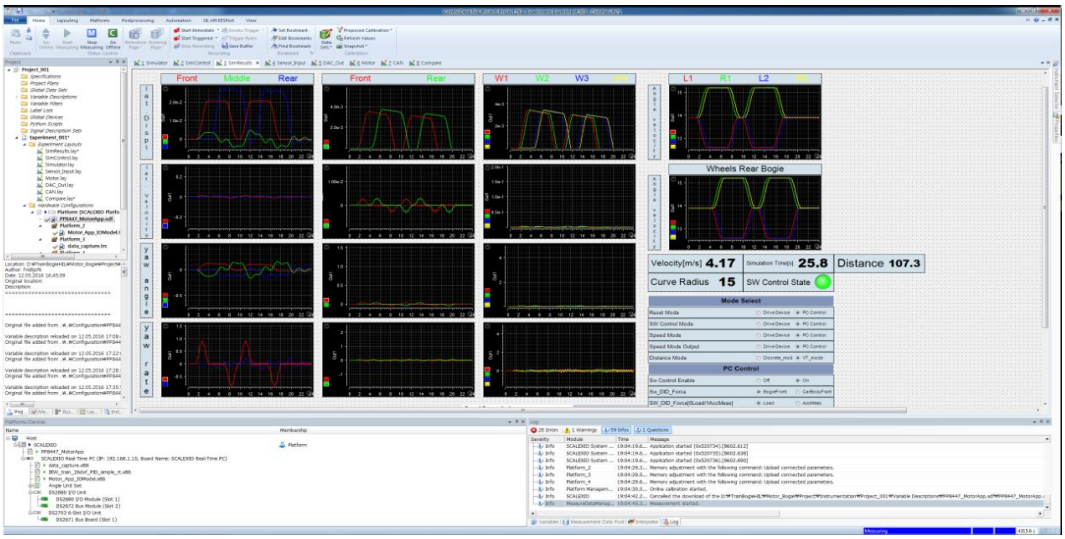

Figure 10. Status monitoring and control variable definition using the control desk

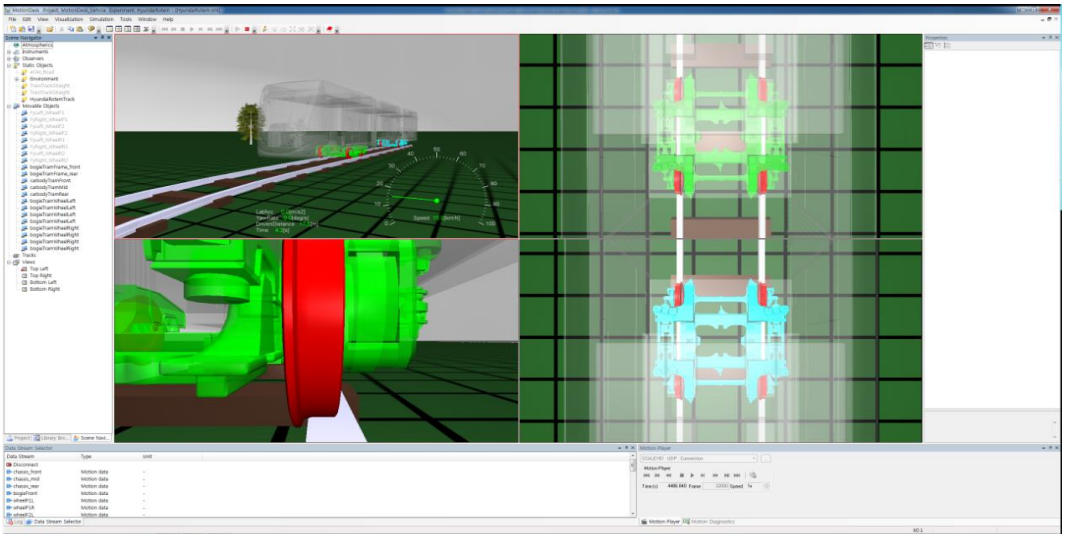

Figure 11. Realization of dynamic characteristics of real-time analysis model using motion desk

3. Controller configuration

Normal railway vehicle uses rigid wheelset, so the restoring force is automatically generated by applying the same traction torque to the left and right sides. However, the independently rotating wheelset can generate restoring force only when independent torque control of the left and right wheels is added in addition to the traction torque.

In this paper, the mechanism for generating IRW's restoring force through individual motor torque control is described, and the lateral displacement and yaw displacement-based restoring control strategies have been verified using HILs.

The lateral displacement-based restoration control strategy is shown in Figure 12. When a left lateral offset occurs (Y_F*-Y_F) in the wheel set, the left wheel torque is increased (T_C*) and at the same time, the right wheel torque is increased (T_C*) in the opposite direction. In this case, a yaw moment in the clockwise direction is generated due to the difference in the left and right wheel torque, thereby generating a restoring force that returns to the center of the rail. On the other hand, when a right lateral offset occurs, the yaw moment in the counterclockwise direction is generated by controlling the restoration torque of the left and right wheels. A similar control strategy can be applied to the yaw displacement of the wheelset caused by the traction torque T_T* that generates the propulsive force of the vehicle under test and the restoring torque T_C* that generates the lateral recovery force.

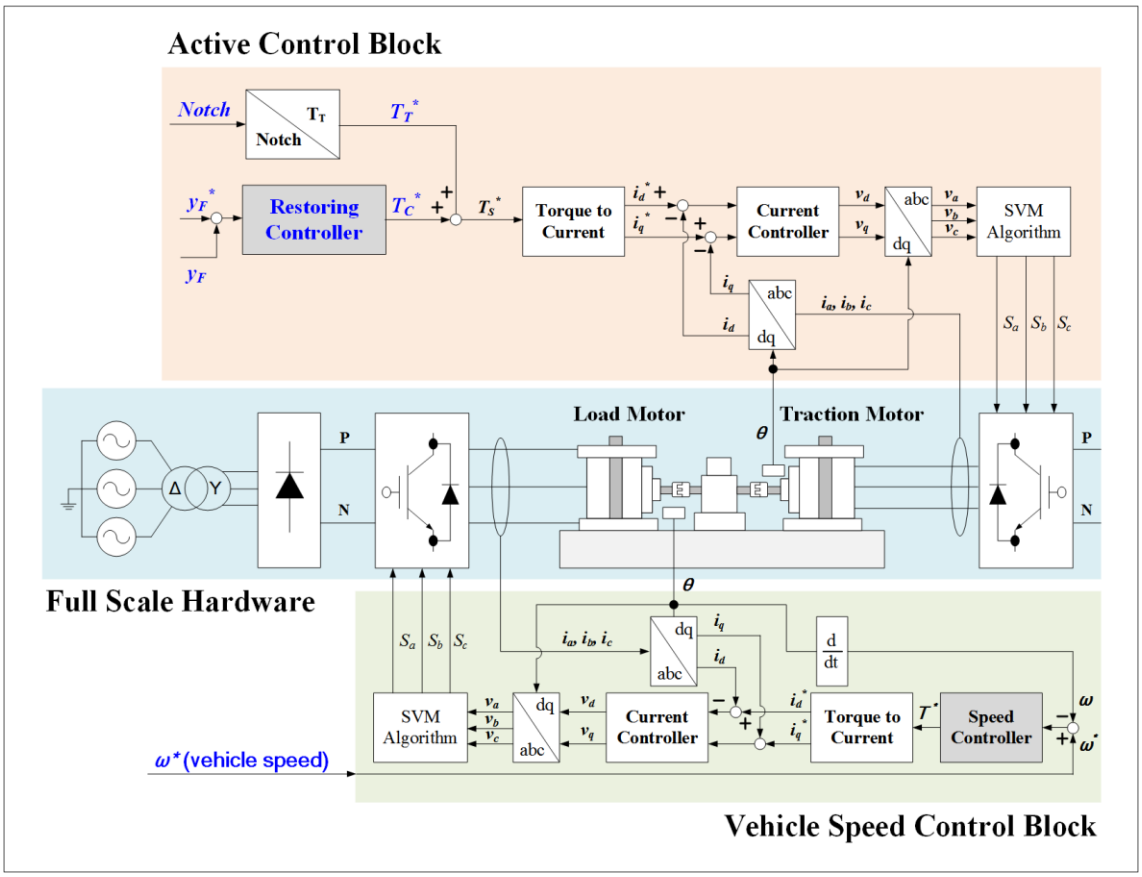

Figure 12. Speed control and restoring active control concept diagram for load motor and traction motor constituting HILs

The configuration of the HILS system for verifying the proposed active control strategy is shown in Figure 13. The entire system consists of a remote-control device (Lever), a real vehicle controller and hardware (inverter + motor for IRWs, inverter + motor for vehicle speed simulation), and RTDS (Real Time Digital Simulator). The remote-control device transmits the traction information (notch information) to the IRWs controller through CAN communication. In RTDS, the

26-degree-of-freedom dynamic equation of a three-module tram is calculated in real time. Among them, the traction torque and recovery torque are controlled by the IRWs controller using vehicle information (lateral displacement and yaw information) calculated in RTDS. The transmitted notch information is converted from the traction controller to the traction torque (T_T*), and the restoring controller feedbacks the lateral displacement of the vehicle and outputs the control torque (T_C*). The IRWs traction motor is controlled with the final torque (T_S*) combined with the traction torque and control torque. The propulsion torque (T_T) and control torque (T_C) information is transmitted to the RTDS to solve the IRWs vehicle equation in real time. At this time, the vehicle speed can be obtained by calculating the longitudinal equation in RTDS using the transferred traction force (T_T). The calculated vehicle speed is input to the vehicle speed control block, which is a load motor control, to simulate vehicle driving. The 26-degree-of-freedom dynamics equation is solved in real time using the transmitted control torque (T_C), and the calculated result includes the lateral or yaw information of the vehicle. This variable is fed back to the vehicle controller to perform restoration control. The calculated state information of the vehicle is mapped to a 3D vehicle model using the real time animation function included in dSPACE's Motion desk program, and implemented to visually check the movement of the actual vehicle.

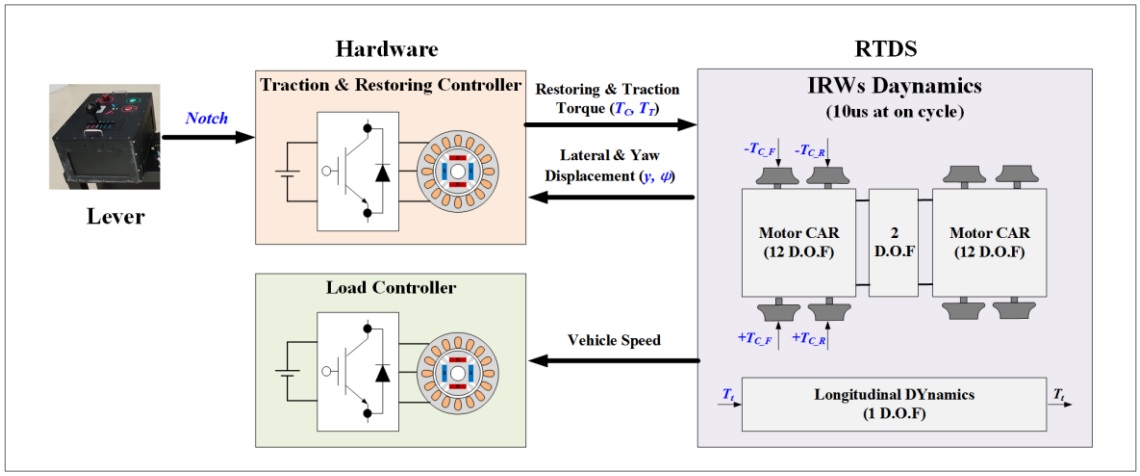

Figure 13. The configuration of the HILS system consists of lever, hardware, and RTDS

4. HILs analysis result

Evaluation of the performance of the resilience control algorithm using individual motor control was performed through real-time experiments under three driving conditions. In particular, it is possible to verify the performance of the development controller in advance before performing the actual driving test through real-time analysis of the same conditions as the test track that is going to proceed with the driving test of the actual test vehicle.

4.1. Analysis with impulse disturbance when running on a straight rail

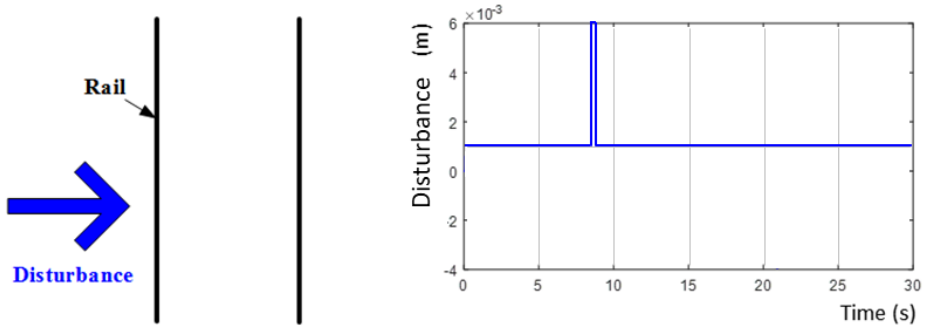

Figure 14. Analysis condition considering lateral disturbance on straight track

First, as shown in Figure 14, the characteristics of the impulse disturbance in a straight section were analyzed. When impulse disturbance is applied in the transverse direction during straight running, displacement occurs in the transverse direction. When the lateral displacement is greatly increased, the wheel flange and the rail are in contact, so the lateral displacement is limited to a maximum of 6.5 mm. Figure 15 shows the phenomenon that the wheel diverges without restoring to the center of the rail even if sufficient time has passed since the disturbance was applied. This shows that the IRWs does not have automatic recovery capability unlike the Rigid wheelset.

The result of adding the lateral displacement-based restoration control proposed in the previous section under the same driving conditions is shown in Figure 16. Since impulse disturbance generates lateral displacement (y), the restoration controller is additionally operated to generate a torque difference on the left and right wheels. Compared to the result in the figure above without resilience control, it can be seen that the wheel is restored to the center after the impulse disturbance input. The result of yaw-based restoring control is shown in Figure 17. After the impulse disturbance is input, the restoration controller operates to reduce the yaw displacement of the wheel set. The lateral displacement-based control is controlled with accompanying vibration, whereas the yaw-based control has a faster recovery control performance and less tendency of vibration than the lateral displacement-based control.

Since the individual motor torque control is performed with the yaw moment using the torque difference of the left and right wheels, it was confirmed that the yaw-based control has superior dynamic characteristics compared to the lateral displacement-based restoring control.

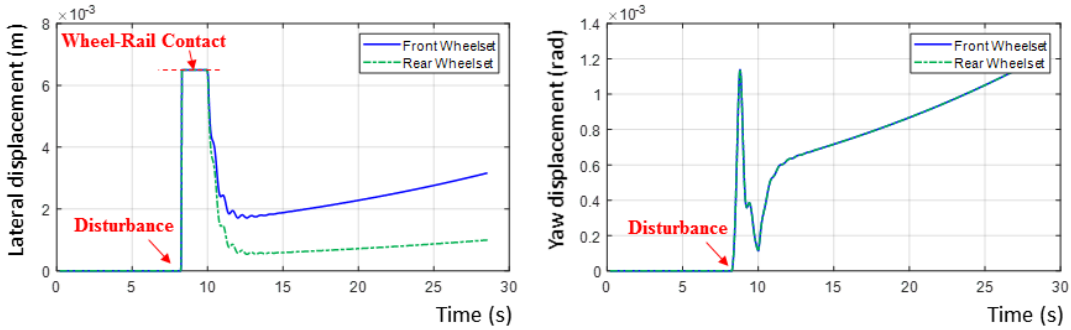

Figure 15. Result graphs without restoration control (lateral displacement, yaw angle)

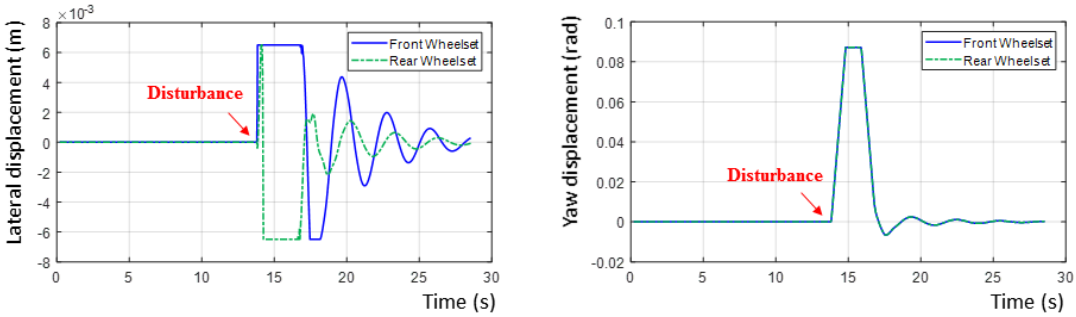

Figure 16. Lateral displacement-based restoration control results (lateral displacement, yaw angle)

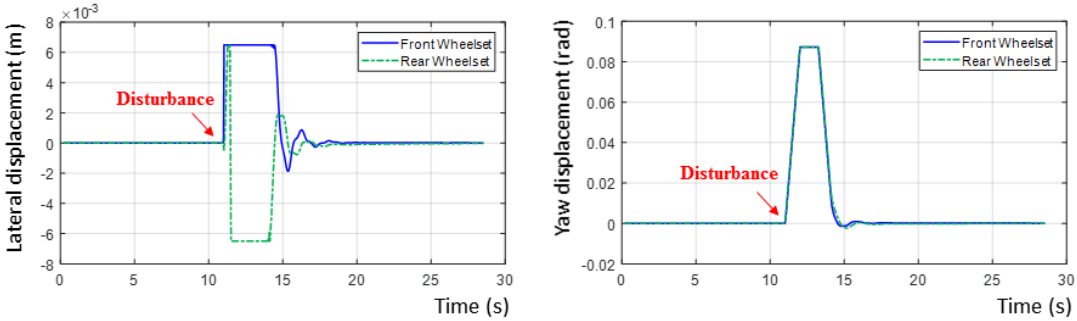

Figure 17. Yaw angle-based restoration control results (lateral displacement, yaw angle)

4.2. Analysis with track irregularity when running on a straight rail

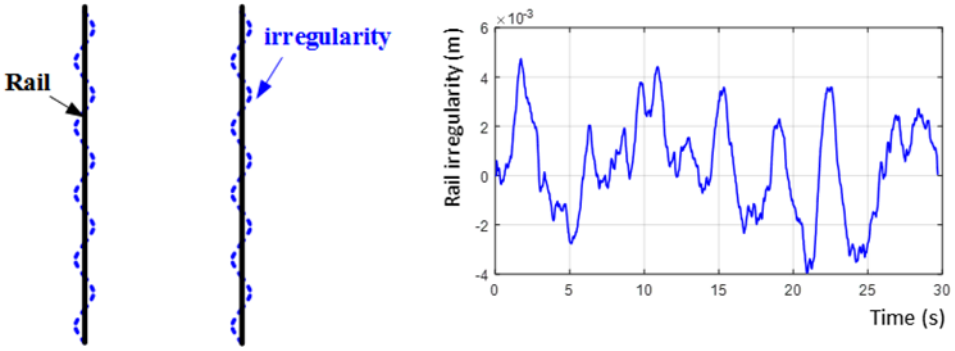

Figure 17. Analysis condition considering rail irregularities on straight track

The actual rail has irregularities as shown in Figure 18. Independent rotating type railway vehicles have insufficient restoring force, so the irregularity of the rail acts small size and high frequency disturbance. As it accumulates, the lateral displacement gradually increases. Therefore, a test was performed to verify the restoration control characteristics for the irregularity of the rail. The irregularity of the rail used in the analysis was measured values of the actual rail. This value was added to the lateral freedom model in the 26-degree-of-freedom vehicle model and configured to act as disturbance. Figure 18 shows the result of performing the restoring control under the given conditions.

Although it is a straight section, the lateral displacement gradually increases before performing the restoration control due to the irregularity of the rail, but the lateral displacement decreases after applying the restoration control. On the other hand, it can be seen that the yaw angle has little improvement effect due to restoring control.

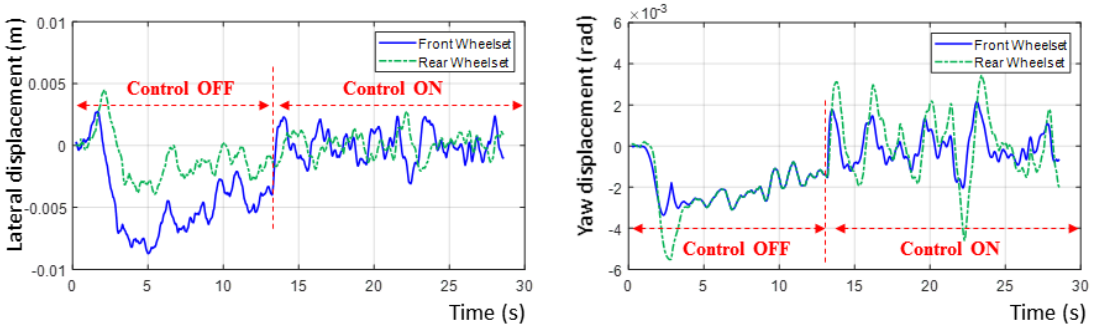

Figure 18. Comparison of control characteristics on straight tracks including track irregularities

4.3. Analysis with real driving track including 15 m curve radius sections

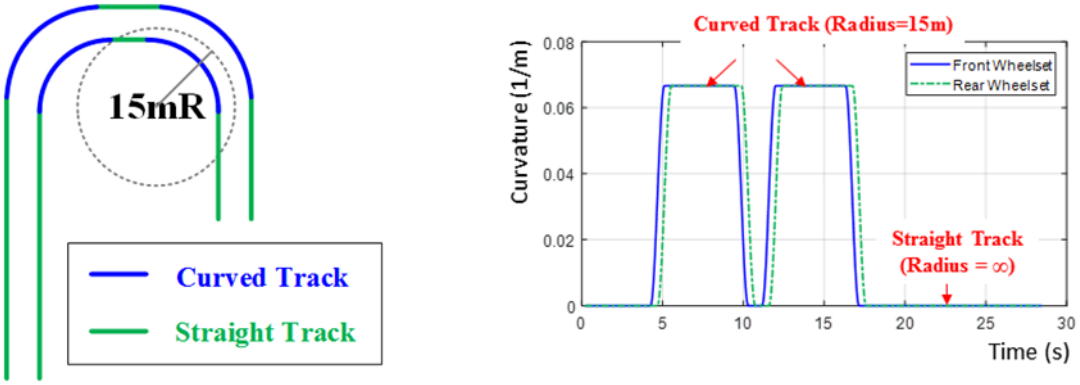

Figure 19. Analysis condition with real test track including 15 m curve radius sections

IRWs (Independently Rotating Wheels) are capable of allowing speed differences between left and right wheels. However, the lateral displacement is largely generated by the vehicle's inertia and centrifugal force when driving in a sharp curve section. A restoring control strategy is applied to improve driving performance when driving on a sharp curve. As shown in Figure 19, the track conditions under which the test run was performed have a mixture of a straight section and a sharp curve sections with radius 15 m. Figure 20 shows the results of running on the test track using only traction control without restoring control. In the straight section, there is no extra disturbance, so it is operated in the center of the rail, and when entering the sharp curve section, lateral displacement is largely generated in the vehicle. It can be seen that the lateral displacement is large while passing through the two sharp curves and the lateral displacement is not restored even after passing the sharp curve sections. The results of applying the proposed restoring control strategy considering motor torque saturation on sharp curve driving are shown in Figure 21. A very large restoration torque is required for restoring control on the sharp curve with a radius of 15 m, but the torque that can be output from the motor is limited. Since the required restoration torque is difficult to generate, sufficient restoration performance is not exhibited when driving on a curved line. In order to verify the validity of the proposed control strategy, the same test was performed without considering the saturation of the output torque of the motor. It was confirmed to secure sufficient control performance as shown in Figure 22. When comparing the test results with Fig. 21, it can be seen that the time between the contact of the flange and the wheel is greatly reduced and restored to the center of the rail. Therefore, it was confirmed that when the proposed restoring torque control was applied, there was room for a significant improvement in the driving stability on a sharp curve than when only the traction torque was controlled.

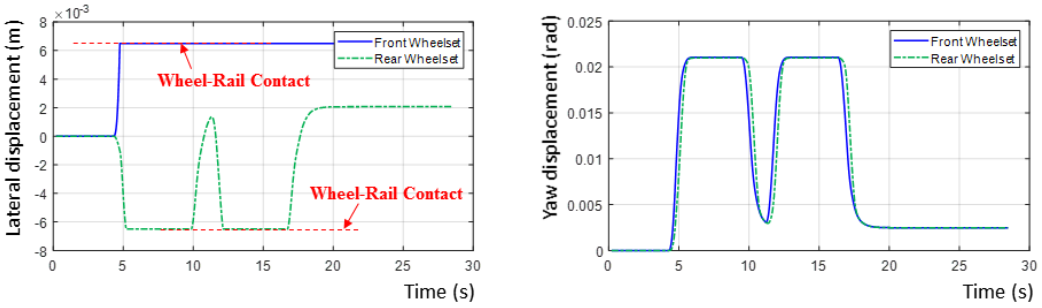

Figure 20. Result graphs without restoration control (lateral displacement, yaw angle)

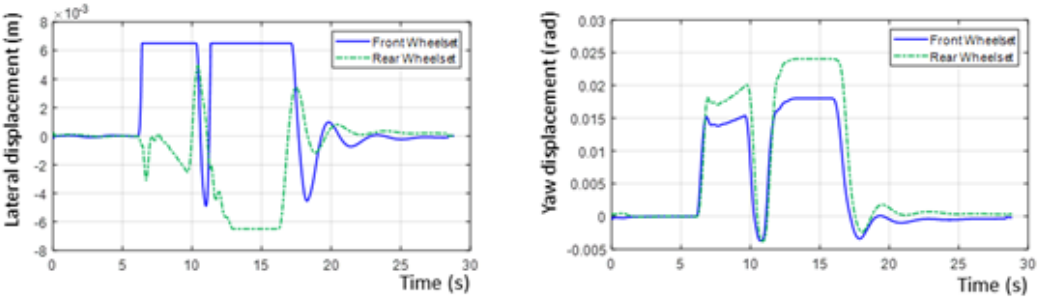

Figure 21. Result graphs considering motor torque limit (lateral displacement, yaw angle)

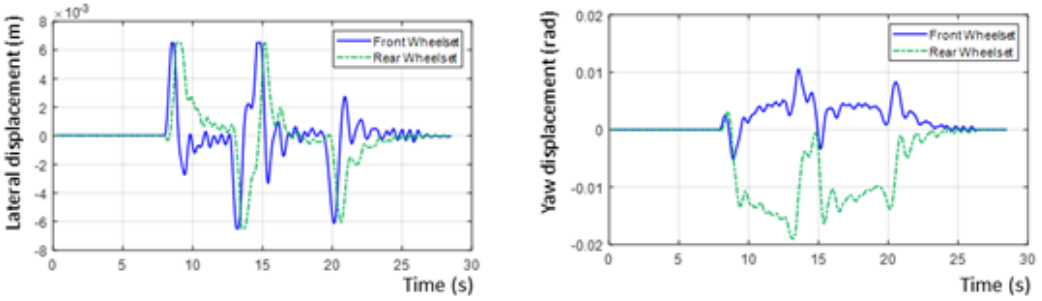

Figure 22. Result graphs without considering motor saturation (lateral displacement, yaw angle)

5. Conclusions

The proposed IRWs restoration control strategy has the advantage that it can be implemented only by changing the soft-ware without adding separate actuators and sensors. The verification of IRWs restoring control strategy using a real vehicle requires a great deal of vehicle manufacturing cost, so most of the verification was performed through analysis using a vehicle's numerical model or through a scaled vehicle and roller rig test. However, these methods have the disadvantage that there are little similarities with actual vehicles. In order to overcome this limitation, this study proposed the HILs system and test method to verify the effectiveness of the restoring control strategy to improve running performance of IRWs.

It was confirmed that the proposed yaw-based restoration control strategy secured better restoration performance than the lateral displacement-based restoration control under impulse disturbance and rail irregularity conditions in straight driving. In addition, the lateral displacement is significantly reduced when restoring force control is performed even in driving conditions that include a sharp curve with 15 m radius. It is expected that the lateral restoration control will improve the sharp curve driving performance, reduce noise and vibration, and prevent serious accidents such as derailment.

The process of verifying the individual motor torque control technology for improving the driving performance of the independently rotating wheel type railway vehicle using HILs is summarized in Figure 23. Based on the SCALEXIO platform, dSPACE's latest real-time analysis computer, a HILs environment was built by connecting the PSMS motor performance test bench and the controller including the inverter with the virtual railway vehicle model.

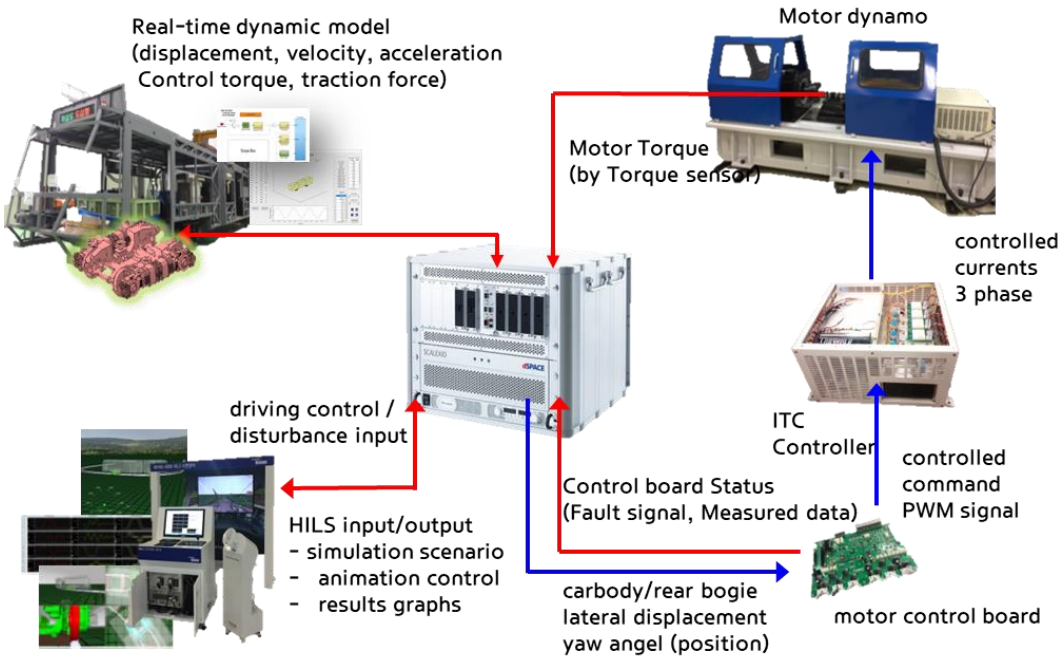

Figure 23. HILs configuration of individual motor torque control technology verification test

Through the developed HILs, a virtual test is performed under a variety of test conditions to secure the stability of the controller and drive motor system, and then a test vehicle for the actual driving test is manufactured, as shown in Figure 24. The driving test and restoration control characteristic evaluation will be conducted. In the case of tests involving risks such as tests considering various failure conditions and abnormal driving conditions even after the actual vehicle driving test is started, additional studies are needed to actively utilize HILs to reduce risk and development time and increase efficiency.

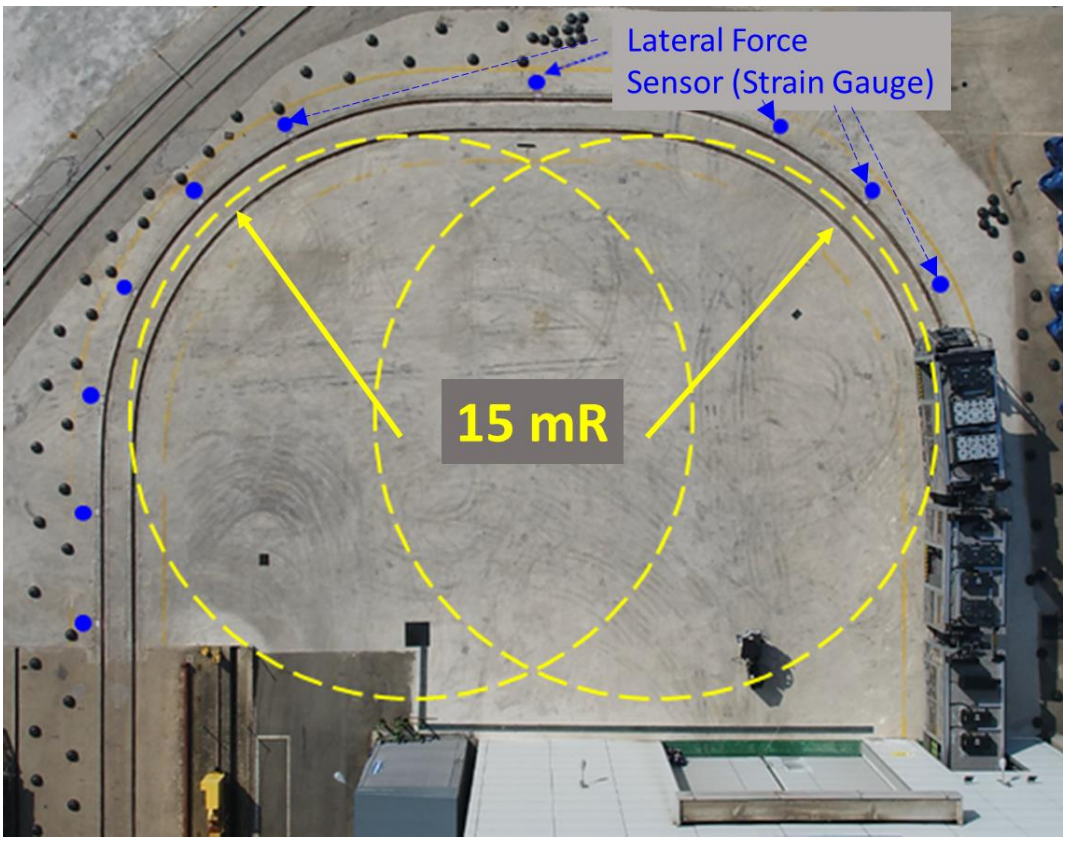

Figure 24. Actual vehicle driving test on sharp curve test line including two 15 m radius curves

References

1. R.V.Dukkipati.; S.Narayana Swamy. Independently Rotating Wheel Systems for Railway Vehicles-A State of the Art Review. *Vehicle System Dynamics*. **1992**, 21, 297-330.
2. R.M.Goodall.; Hong.Li. Solid Axle and Independently Rotating Wheelsets - A Control Engineering Assessment of Stability. *Vehicle System Dynamics*. **2000**, 33, 57-67.
3. Y.Cho.; J.Kwack. Development of a New Analytical Model for a Railway Vehicle Equipped with Independently Rotating Wheels. *IJAT*. **2012**, 13(7), 1047-1056.
4. H.Ahn.' H.Lee. S.Go. Y.Cho. J.lee. Control of the Lateral Displacement Restoring Force of IRWs for Sharp Curved Driving. *Journal of Electrical Engineering & Technology*. **2016**, 11(4), 1041-1048.
5. Y.Oh.; Y.Cho. I.Kim. J.Lee. H.Lee. Restoring Torque Control Strategy of IPMSM for the Independently Rotating Wheelsets in Wireless Trams. *Journal of Electrical Engineering & Technology*. **2017**, 12(4), 1683-1689.
6. J.Won.; Y.Oh. J.Lee. H.Ahn. H.Lee. Y.Cho. A Study on the Individual Control Method Comparing the Lateral Displacement Control of Front Wheel and Rear Wheel of IRWs System. *IEEE Transaction on Applied Superconductivity*. **2018**, 28(3), 1-5.
7. T.X.Mei.; H.Li. Control Design for the Active Stabilization of Rail Wheelsets. *Journal of Dynamic Systems Measurement and Control*. **2008**, 130, 0110021-9.
8. T.X.Mei.; R.M.Goodall. Robust Control for IRW on a Railway Vehicle Using Practical Sensors. *IEEE Transactions on Control System Technology*. **2001**, 9(4), 599-607.
9. J. Perez.; J.M.Busturia. T.X.Mei. J.Vindas. Combined active and traction for mechatronic bogie vehicle with independently rotating wheels. *Annual Review in Control*, **2004**, 28, 207-214.
10. M.Gretzschel.; L.Bose. A New Concept for Integrated Guidance and Drive of Railway Running Gears. *Vehicle System Dynamics*. **2002**, 10, 1013-1028.
11. T.X.Mei.; R.M.Goodall. A.H.Wickens. Dynamic and Control Assessment of Rail Vehicle Using Permanent Magnet Wheel Motor. *Vehicle System Dynamics Supplement*. **2002**, 37, 326-337.
12. J.Li.; R.M.Goodall. T.X.Mei. H.Li. Steering Controllers for Rail Vehicles with Independently Driven Wheel Motors. *Electronic System and Control Division Research*. **2003**, 4-6.

13. J.Feng.; J.Li. R.M.Goodall. Integrated control strategies for railway vehicles with independently-driven wheel motors. *Front. Mech. Eng. China*. **2008**, 239-250.
14. G.Kim.; J.Kim. J.Jeon. S.Kim. E.Kim. J.Lee. M.Park. I.Yu. Hardware-in-the-loop Simulation Method for a Wind Farm Controller Using Real Time Digital Simulator. *Journal of Electrical Engineering & Technology*. **2014**, 9(5), 1489-1494.
15. J.Wang.; A long short-term memory neural network approach for the hardware-in-the-loop simulation of diesel generator sets. *Measurement and Control*. **2019**, 53(1-2), 229-238.
16. G.Kumar.; P.Kaliannam. S.Padmanaban. J.Nielsen. F.Blaabjerg. Effective Management System for Solar PV Using Real-Time Data with Hybrid Energy Storage System. *Applied science*. **2020**, 10, 1-15.
17. J.Yoon.; S.Lee. J.Bin. Y.Kong. S.Lee. The Modeling and Simulation for the Design Verification of Submarine Charging Generator by using Real-Time Simulator. *ICPE*. **2011**, 5, 1406-1410.
18. Y.Nam.; H.Jang. S.Hong. S.Park. Fault Detection System Design and HILS Evaluation for the Smart UAV FCS. *International Journal of Control Automation and System*. **2007**, 5(1), 104-109.
19. Y.Lai.; W.Ting. Design and Implementation of an Optimal Energy Control System for Fixed-Wing Unmanned Aerial Vehicles. *Applied science*. **2016**, 6, 1-24
20. K.Park.; S.Heo. Development of Hardware-in-the-Loop Simulation System for Use in Design and Validation of VDC logics. *International Journal of Precision Engineering and Manufacturing*. **2003**, 4(3), 28-35.
21. K.Lee.; J.Jeon. D.Hwang. Y.Kim. S.Lee. Design of Antilock Brake Controller using Real-Time Dynamics Simulation System. *ICPE*. **2004**, 10, 251-254.
22. M.Yoon.; W.Lee. M.Sunwoo. Development and Implementation of Distributed Hardware-In-the Loop Simulator for Automotive Engine control System. *IJAT*. **2005**, 3, 107-117.
23. S.Kim.; H.Jung. J.Shim. C.Kim. Development of Vehicle Dynamics Model for Real-Time Electronic Control Unit Evaluation System Using Kinematic and Compliance Test Data. *IJAT*. **2005**, 12, 599-605.
24. H.Jo.; U.Lee. S.Kam. Development of the Independent-Type Steer by Wire System Using HILS. *IJAT*. **2006**, 5, 311-317.
25. S.Lee.; K.Park. T.Hwang. J.Hwang. Y.Jung. Y.Kim. Development of Hardware-In-the-Loop Simulation System as a Testbench for ESP Unit. *IJAT*. **2007**, 4, 203-209.
26. D.Song.; L.Li. X.Zeng. S.Li. G.Li. G.Li. H.He. X.Li. Hardware-in-the-loop validation of speed synchronization controller for a heavy vehicle with hydraulic drive system. *Advances in Mechanical Engineering*. **2018**, 10(4), 1-15.
27. G.Xu.; P.Diao. X.He. J.Wu. G.Wang. C.Wang. Research on vehicle active steering control based on linear matrix inequality and hardware in the loop test scheme design and implement for active steering. *Advances in Mechanical Engineering*. **2019**, 11(11), 1-12.
28. H.Yeo.; C.Song. C.Kim. H.Kim. Hardware in the Loop Simulation of Hybrid Vehicle for Optimal Engine Operation by CVT Ratio Control. *IJAT*. **2004**, 9, 201-208.
29. S.Han.; J.Lim. Performance Assessment of a Lithium-Polymer Battery for HEV Utilizing Pack-Level Battery Hardware-in-the-Loop Simulation System. *Journal of Electrical & Technology*. **2013**, 11, 1431-1438.
30. Z.chen.; X.Zhou. Z.Wang. Y.Li. B.Hu. A Novel Emergency Braking Control Strategy for Dual-Motor Electric Drive Tracked Vehicles Based on Regenerative Braking. *Applied science*. **2019**, 9, 1-22.
31. C.Huang.; F.Lei. X.Han. Z.Zhang. Determination of modeling parameters for a brushless DC motor that satisfies the power performance of an electric vehicle. *Measurement and Control*. **2019**, 52(7-8), 765-774.
32. C.Kang.; Analysis of the Braking System of the Korean High-Speed Train Using Real-Time Simulation. *Journal of Mechanical Science and Technology*. **2007**, 21(7), 1048-1057.
33. D.Lee.; C.Kang. A mechanical brake hardware-in-the-loop simulation of a railway vehicle that accounts for hysteresis and pneumatic cylinder dynamics. *Advances in Mechanical Engineering*. **2015**, 7(11), 1-11.
34. Y.Jeong.; G.Ahn. K.Ko. Evaluation Method of Tram Signal Priority Strategy Using HILS. *Journal of the Korean Society for Urban Railway*. **2018**, 6(1), 9-15.